J. Marine Sci. Appl. (2012) 11: 134-142
DOI: 10.1007/s11804-012-1115-4

Analysis of the Comprehensive Physical Field for a New Flywheel Energy Storage Motor/Generator on Ships

Yali Yu[1,2*], Yuanxi Wang[1], Guosheng Zhang[1] and Feng Sun[2]

1. Research Institute of Energy Storage Technology and Application, Harbin Engineering University, Harbin 150001, China
2. Department of Automation, Harbin Engineering University, Harbin 150001, China

Abstract: A novel flywheel energy storage (FES) motor/generator (M/G) was proposed for marine systems. The purpose was to improve the power quality of a marine power system (MPS) and strengthen the energy recycle. Two structures including the magnetic or non-magnetic inner-rotor were contrasted in the magnetostatic field by using finite element analysis (FEA). By optimally designing the size parameters, the average speed of FEA results of was 17 200 r/m, and the current was controlled between 62 and 68 A in the transient field. The electrical machine electromagnetism design was further optimized by the FEA in the temperature field, to find the local overheating point under the normal operation condition and provide guidance for the cooling system. Finally, it can be concluded from the comprehensive physical field analysis that the novel redundant structure M/G can improve the efficiency of the M/G and maintain the stability of the MPS.

Keywords: marine power system; flywheel energy storage; Halbach array magnet structure; comprehensive physical field; motor/generator; finite element analysis
Article ID: 1671-9433(2012)01-0134-09

1 Introduction

Energy storage is an important aspect of realizing energy saving, emission reduction, and sustainable development. It can increase energy efficiency and solve energy crises. Since energy crises have an adverse effect on the world economic development process, all countries must face the challenging problem of energy storage. There are four main ways to store energy: pumped storage, storage battery, ultracapacitor, and flywheel energy storage (FES). In contrast with other methods, FES has the advantages of long service life, high power density, and large energy storage densities which are not limited by the times of charging and discharging and do not harm the environment, as seen in Tang (2009) and Tang (2003). Therefore, FES is the most promising new kind of energy storage technology.

The FES system is a mechanical device which stores electrical energy in the form of kinetic energy. The magnetic suspension system, motor/generator (M/G), and flywheel rotor make up the key components of the FES system to realize the process of energy input, storage, and output. The modern FES system with high-capacity and extended storage capabilities was first developed in the 1950s but was limited by the technical conditions; it was not developed widely at that time. The FES technique entered into a new high-speed development stage in the 1990s. Now it is used in wind power generators, electromagnetic cannons, uninterruptible power supplies (UPS), and power grid peak regulations, as seen in Wang (2008). Especially in the field of marine science, it has the advantage of easy installation and integration of the motor and generator because of its outstanding contribution to improving marine power systems.

2 The structural design of the flywheel energy storage motor/generator

The M/G and its control system is the core dynamic component of energy conversion in an FES device. The M/G must combine the characteristics of a high efficiency motor and generator in order to reverse. So far, there are three types of electrical machines that have been widely applied: the induction electrical machine, as in Ckdenas *et al.* (2000) and Kato *et al.* (2009), reluctance electrical machine, as in Park *et al.* (2008) and Rajapakshe *et al.* (2008), and permanent magnet PM electrical machine, as in Kohari (2009) and Upadhyay and Mohan (2009), Yu *et al.* (2009). Among them the PM electrical machine, especially the Halbach magnetized structure, is the most widely used M/G with the characteristics of small volume, fewer losses, high efficiency and power densities, high torque output ability, as well as lower mass and highly reliable operation, as demonstrated in Jang *et al.* (2009).

In this study, the PM brushless M/G has been chosen as a prototype. The 3-D model of the flywheel with the M/G and the profile view of the M/G are shown in Fig.1.

Received date: 2011-09-27.
Foundation item: Supported by the Fundamental Research Funds for the Central Universities under Grants Nos. HEUCF101706 and HEUCF111705.
***Corresponding author Email:** yuyali2000@126.com

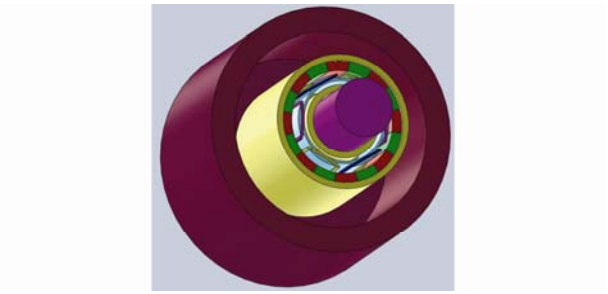

(a) The 3-D model of the flywheel and M/G

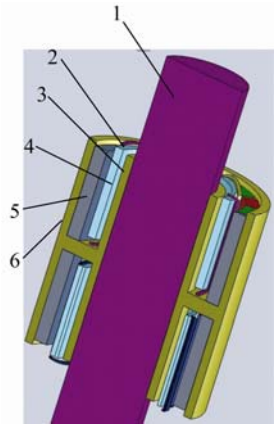

1. Shaft;
2. Coil;
3. Inner-rotor core;
4. Winding insulation and skeleton;
5. PM;
6. Outer-rotor core

(b) The profile view of the M/G

Fig.1 The 3-D M/G structure

2.1 The permanent magnet (PM) structure

The air-gap magnetic field of a Halbach magnetized structure PM brushless M/G is sine. Additionally, the sine waveform electromotive force (EMF) can be obtained. The manufacturing angle of the Halbach structures can be divided into the whole ring-form Halbach array and the subsection Halbach array, as in Zhu and Howe (2001) and Xia *et al.* (2004). Without particular windings and slot structure, the ring-form Halbach array can obtain the sine form no-load EMF. However, it is difficult to manufacture and has been limited by the machining process. The subsection Halbach array consists of many blocks, and a higher number of blocks can lead to an ideal Halbach magnetized structure while on the other hand increasing the processing cost. The prototype of a PM brushless M/G has four poles, and every pole has been partitioned to four blocks. Through the optimized design, the subsection Halbach array magnet structure can obtain higher air-gap magnetic flux density. It can reduce the volume of motor, weight, and inertia and improve the dynamic performance of the M/G which can also improve the utilization rate of the PM material. The torque ripple is small, as in Zhu *et al.* (2000).

2.2 Double-rotor core structure

The novelty of this electrical machine model is the rotor core which has been designed for the special "H" form structure; both the axial up-down and radial the inner-outer are all double. The structure can fully use the PM, greatly reduce the volume, and improve the motor power density, which is most helpful for realizing high speed operation in an FES system.

2.3 Stator skeleton, coils, and drive mode

The stator is ironless in order to reduce the iron losses and improve the efficiency of the electrical machine. The windings have been winded in the stator skeleton which is made of epoxy. Stator windings are made up of six coils and with the four poles forming the fractional slot. Compared with the integer slot, they have the following advantages:

1) Reducing the slot insulation space and simplifying the embedding technology;

2) Reducing the amount of the copper, lowering the cost, and improving working efficiency;

3) Improving the back EMF waveform and decreasing the load torque ripple;

4) Reducing the temperature rise.

The drive control circuit adopts two-phase breakover and three-phase six-state star form windings.

The PM brushless M/G prototype with the structure of a double-rotor and ironless stator is comprised of the following components from inside to outside: the shaft, inner rotor core, stator skeleton, winding, permanent magnet, and outer rotor core (the distance from the sampling circle to inner diameter of the permanent magnet is 3 mm). The overall magnetic performance of the prototype has been significantly affected by the structure sizes such as the PM thickness, the air gap length, and the inside and outside of the core layer thickness. There are two types of double-rotor structures including the double-rotor all magnetic structure and the only outer-rotor magnetic structure. Using the FEA method, the key parameters of the two types will be calculated in a static magnetic field in the next section in order to obtain the optimal structure size parameters.

3 Contrast of the inner-rotor magnet in the magnetostatic field

The Halbach magnet array has the characteristic of strengthening one magnetic field and weakening another side. The out-rotor prototype M/G is the inner magnetic field, so the PM inner field is strong, as in Zhu and Yan (2008). Lines of magnetic force are crowded and the flux density at the air gap is high. The approximate sine wave air-gap magnetic flux density can be obtained, as seen in Jang and You (2008).

3.1 The analysis of the M/G prototype of which the double-rotor core is all magnetic

The structure of the double-rotor is all magnetic, and the parameters of the key structure size have been calculated by using the FEA at the 2-D magnetostatic field. The following different variables have been set to optimized parameters:

the inner-rotor thickness, air gap length, PM thickness, thickness of the out-rotor core. These variables' names are known as R_1, L_{gap}, L_{mag}, R_2, respectively. Every step of each optimization parameter is 2 mm; the total number of samples is three.

The results of FEA are shown in Fig.2 where it can be seen that the effect on the air-gap flux density (which is represented as B_r) by PM thickness and the air gap length is most obvious. Air-gap flux density increases as the PM thickness increases and the length of the air gap decreases. The increasing of the air gap flux density is approximately equal when the increase amplitude of each length is the same. Air-gap flux density is directly proportional to the inner-rotor core thickness. Although air-gap flux density increases with the increase of the inner-rotor core length, to a certain extent the increasing amplitude slows down. When the inner-rotor core thickness is greater than 5 mm, its effect on the air-gap flux density weakens gradually. The thickness of the outer-rotor core has no effect on the magnetic field or the varying thickness of the outer-rotor core; the six curves nearly coincide with each other. From the harmonic component figures transferred by the fast Fourier method it can be seen that the fundamental component is high of the Halbach array magnet structure, while by contrast the harmonic component is low, Yu and Wang (2011a).

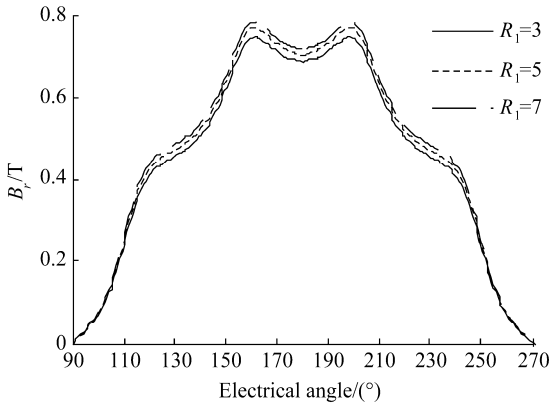

(a) The air gap flux density changes with inner-rotor length

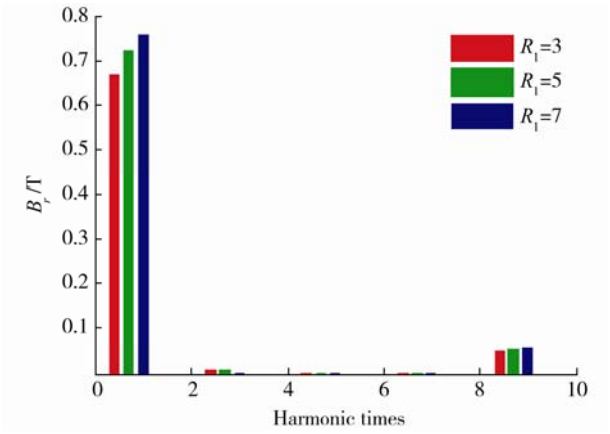

(b) The FFT curves of (a)

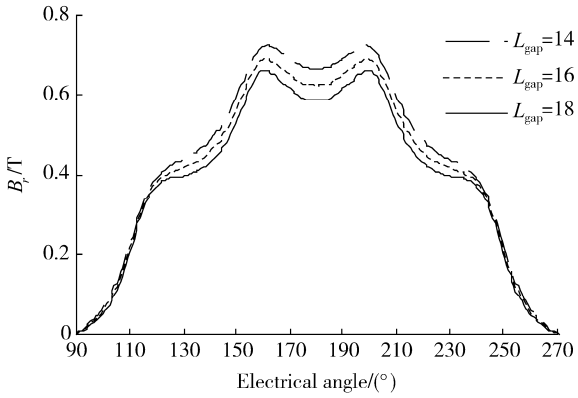

(c) The air gap flux density changes with the air gap length

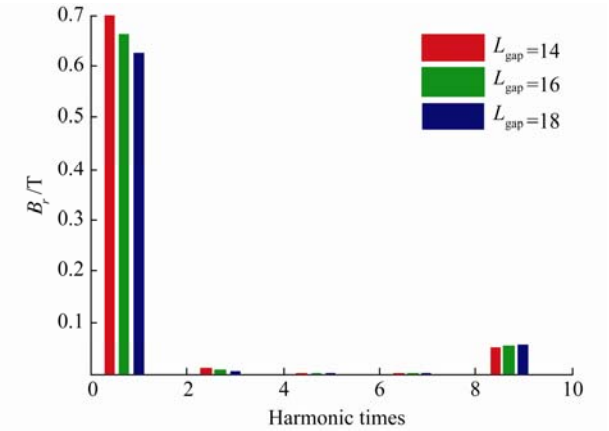

(d) The FFT curves of (c)

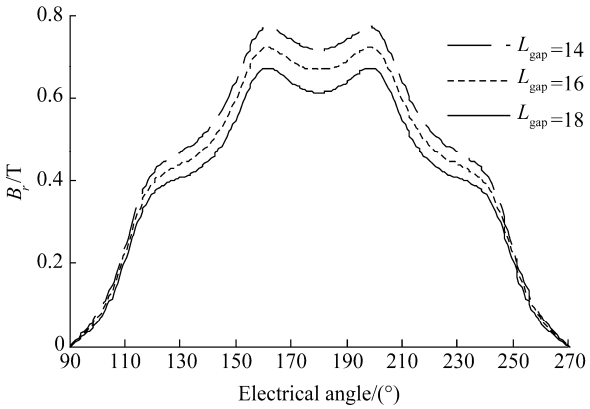

(e) The air gap flux density changes with the magnet length

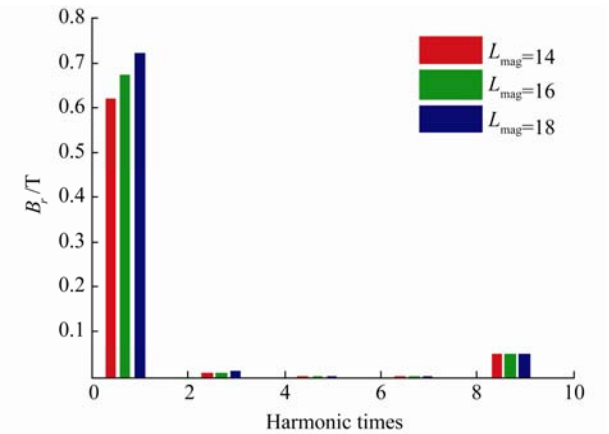

(f) The FFT curves of (e)

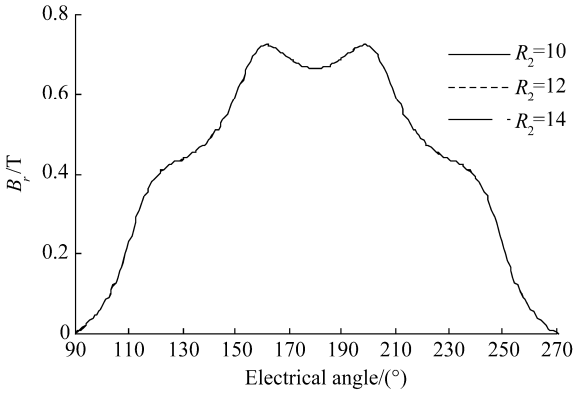

(g) The air gap flux density changes with outer-rotor length

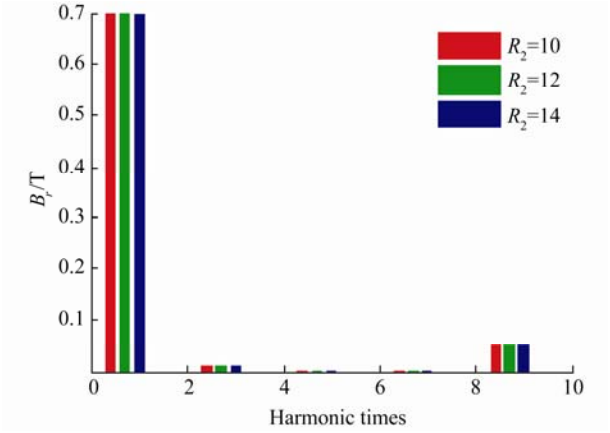

(h) The FFT curves of (g)

Fig.2 The calculation of the key parameters of the double-rotor all magnetic

3.2 The analysis of the M/G prototype in which only the outer-rotor core is magnetic

When the structure of only the outer-rotor core is magnetic, the parameters of the key structure size have been calculated by using FEA in the 2-D magnetostatic field. The definition of specific parameters is the same as in the last section.

The results of FEA are shown in Fig.3. It can be seen that the PM thickness has an effect on the air-gap flux density. Air-gap flux density increases when the PM thickness increases, and its increase is approximately equal if the increase amplitude is the same. Air-gap flux density increases with the decrease of the air gap length and the inner-rotor core thickness, and its decrease is approximately equal if the increase amplitude of the air gap length or the inner-rotor core thickness is the same, respectively. As the M/G structure of the core is all magnetic, the thickness of the outer-rotor core has no effect on the magnetic field or different thicknesses of the outer-rotor core; the six curves nearly coincide with each other. From the harmonic component figures transferred by the fast Fourier method it can be seen that there is not a third, fifth, or seventh but only a ninth harmonic component, which is the same as the structure in the scenario where the double-rotor core is all magnetic, Yu and Wang (2011b).

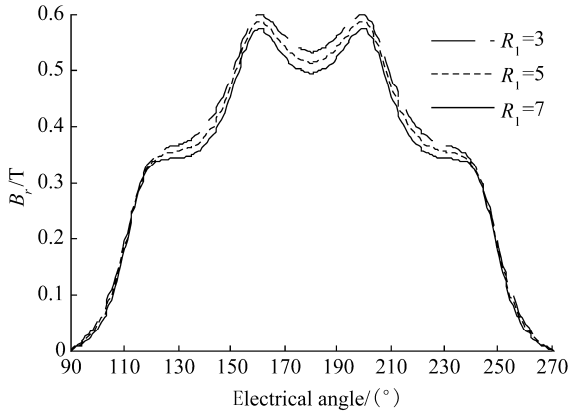

(a) The air gap flux density changes with inner-rotor length

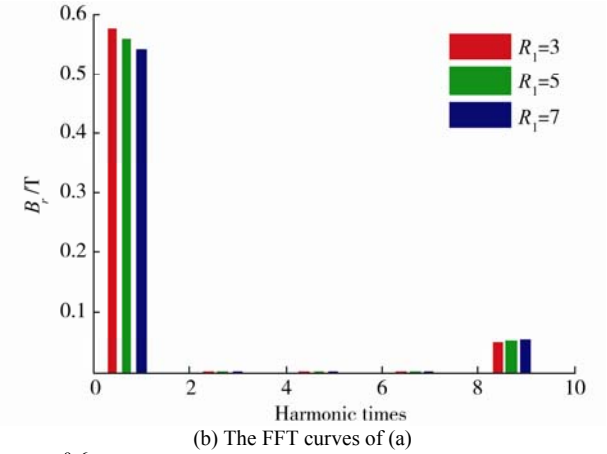

(b) The FFT curves of (a)

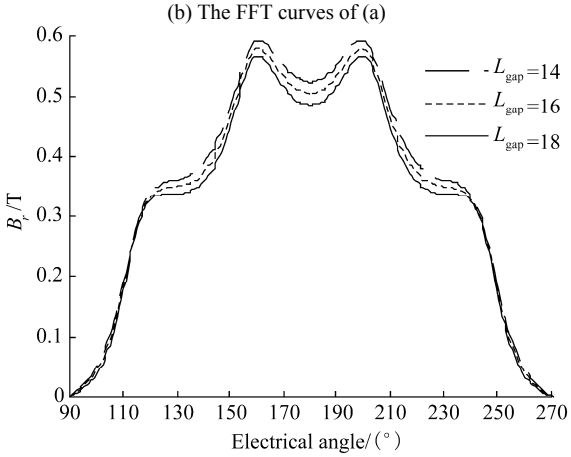

(c) The air gap flux density changes with the air gap length

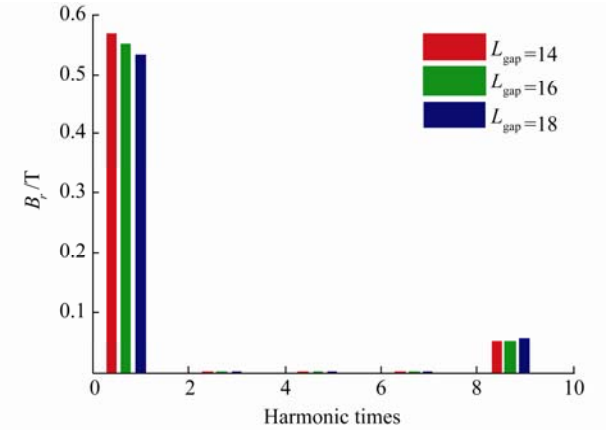

(d) The FFT curves of (c)

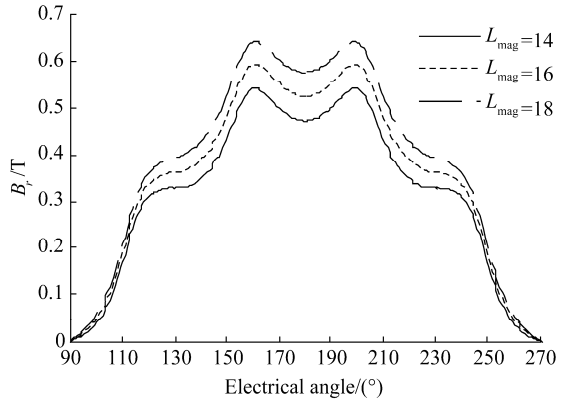

(e) The air gap flux density changes with the magnet length

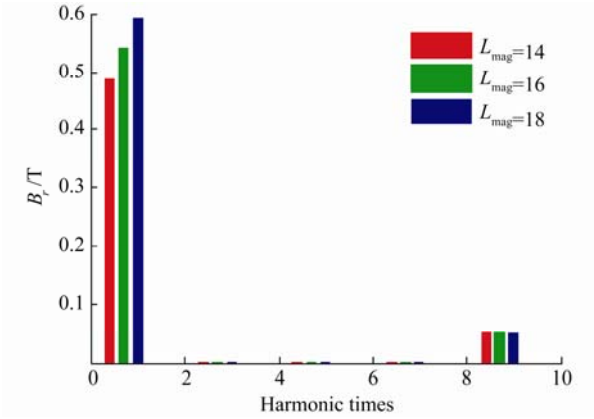

(f) The FFT curves of (e)

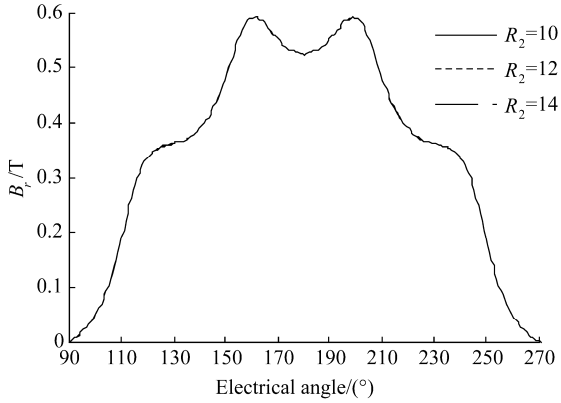

(g) The air gap flux density changes with outer-rotor length

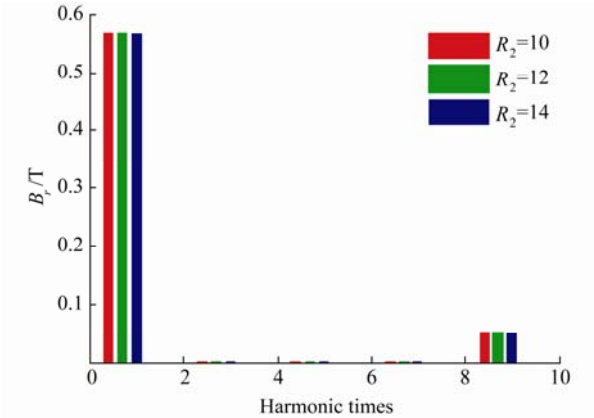

(h) The FFT curves of (g)

Fig.3 The calculation of the key parameters in the scenario that only the outer-rotor is magnetic

In the same way, as seen in the above analysis on the key parameters, the air-gap flux density of the Halbach array structure in a scenario where the double-rotor core is all magnetic is higher than when only the outer-rotor core is magnetic. From the standpoint of numerical value, the former has more advantages. On the other hand, the FES requests high speed, high power, and small volume, and the overtopping air gap flux density is not better than the performance when only the outer-rotor core is magnetic. When only the outer-rotor core is a magnetic structure, the increase of the air-gap length has little effect on the flux density magnitude. Air-gap flux density is inversely proportional to the inner-rotor core thickness; for this reason, reducing the inner core thickness reduces the total volume and causes the flux density to increase only a little.

4 The transient field calculation for the Halbach array magnet structure

According to the index of the prototype M/G (power 7.5 kW, rate speed 17 000 r/m, moment of inertia 2.19 kg/m^2), the structure parameters are 4/6 (poles/slots), the Halbach array is magnetized, and each magnet has 4 blocks. The key electrical parameters are as follows: the DC bus voltage is 110 V, the current is 70 A, the drive controller uses the current amplitude limiting, the maximum and the minimum of the hysteresis loop are 68 and 62 A.

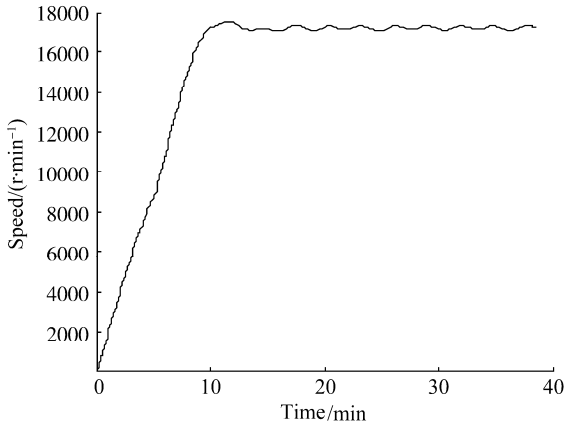

Fig.4 Transient field speed curve

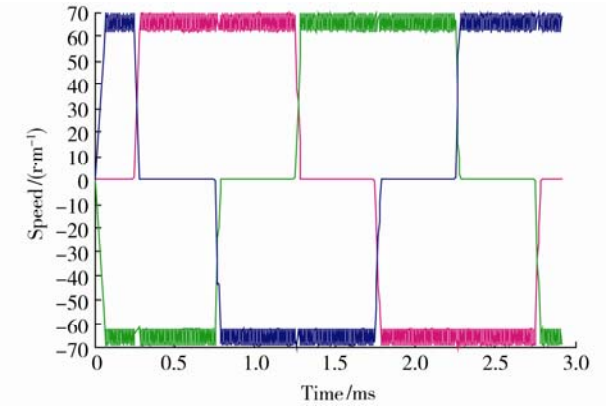

Fig. 5 Transient field current curve

Through the FEA calculation of the model of the M/G in the 2-D transient field, the speed curve has been obtained and is shown in Fig.4. The average speed is 17 100 r/m. With the large moment of inertia at 2.19 kg/m^2, the FES system starting time is very time consuming with a rise time of about 15 minutes until the speed reaches the steady state. The stable speed curve produces fluctuation and its amplitude is less than 120 r/m which is caused by the current limiting and drive current commutation. The current curve is shown in Fig.5 from which it can be seen that current limiting has controlled the current in the range of positive and negative 62–68 A. Limiting the lower current can ensure the electrical machine torque output capacity and improve the rise time of speed. Limiting the larger current can reduce the armature thermal load of the electrical machine while reducing the armature current density and the armature copper losses. It also can avoid excessive current which can cause large losses, then large calorific power which makes the PM demagnetization and reduces electrical performance, even leads to a serious problem of burning the power devices of the drive.

5 The transient temperature field calculation for the Halbach array magnet structures

Through using the FEA method the actual parameters are calculated in the transient field for the M/G prototype in the previous section, and both the speed and the current basic parameter curves are obtained. Then by simulating in the temperature field, for the purpose of further optimizing the electromagnetic design the electrical machine local overheating points that can provide guidance for the cooling system have been found.

5.1 Loss analysis

Because the M/G has a high speed, small volume, and high power density, it has caused large losses per unit volume. To calculate temperature accurately is not only a key problem for the high-speed electrical machine design, but also the necessary preparation for its temperature field analysis and calculation. In the high frequency electro-magnetic field, alternating current produces a skin effect and proximity effect; both effects will cause the windings' copper losses to increase. The additional losses caused by the skin effect and proximity effect have been defined as eddy current losses; both the eddy current losses and DC losses are called AC losses, as in Wasaki *et al*. (2009) and Xi and Sullivan (2009), among which the iron losses make up a large portion. The principle of the generation of the iron losses is more complex. There are alternating and rotating magnetic fields in the electrical machine simultaneously. The alternating iron losses and rotating iron losses are generated by the two fields respectively. In different magnetic fields the ratio of each is different. So in the sense of numerical calculation, it is very difficult to accurately calculate the core losses. The following reasons will cause the eddy current losses: the magnetic motive force due to the stator armature current, the uneven distribution of the air gap magnetic conductance, and the higher harmonic component of the main PM. These factors will cause the temperature rise of PM, the change of magnet performance, and then influence the efficiency and operation performance of electrical machines. The main losses of the redundant Halbach PM brushless M/G in this paper are PM eddy current losses, iron losses, and the windings' copper losses. But due to the frequency of the prototype, the M/G electromagnetic field is only 0.5k; the skin effect and proximity effect have been ignored when calculating the windings copper losses which are caused by a high frequency electromagnetic field. PM eddy current losses and iron losses are calculated in the 2-D transient field.

5.2 The transient temperature field calculation

The FEA method is employed to achieve the simulation for the prototype M/G in the transient temperature field under natural conditions, only considering the conduction and convection heat transfer and while ignoring the thermal radiation effect. Therefore, according to the heat transfer theory, the transient 3-D heat conduction equations can be written as:

$$\begin{cases} K_x \dfrac{\partial^2 T}{\partial x^2} + K_y \dfrac{\partial^2 T}{\partial y^2} + K_z \dfrac{\partial^2 T}{\partial z^2} + q = c\gamma \dfrac{\partial T}{\partial \tau} \\ -K \dfrac{\partial T}{\partial n}\Big|_{s_1} = 0 \\ -K \dfrac{\partial T}{\partial n}\Big|_{s_2} = \alpha (T - T_e) \end{cases} \tag{1}$$

where, T is temperature; K_x , K_y , K_z are the thermal conductivities of each medium in the directions of x , y , z ; q , c , γ are the heat source density, thermal capacity and density, respectively; τ is the time; S_1 and S_2 are the thermal insulation boundary surface and heat radiation boundary surface; T_e and α are temperature of the ambient mediums and heat radiation coefficient of S_2 surface; K is the thermal conductivity coefficient of S_1 and S_2 surface normally.

Through mathematical analysis, the equivalent transformation corresponding to the equation first can be rewritten as:

$$F(T) = \frac{1}{2}\iiint_{\Omega}\left[K_x\left(\frac{\partial T}{\partial x}\right)^2 + K_y\left(\frac{\partial T}{\partial y}\right)^2 + K_z\left(\frac{\partial T}{\partial z}\right)^2\right]\mathrm{d}\Omega + \iiint_{\Omega}\left(\frac{c\gamma}{2}T\frac{\partial T}{\partial t} - qT\right)\mathrm{d}\Omega + \frac{1}{2}\alpha\int_{S_2}(T - 2T_e)T\mathrm{d}s \tag{2}$$

The prototype is axially symmetric so that the middle of axis does not have thermal exchange. As its circumferential

structure is repeated periodically and considering the effect of the windings end, take two half-turn windings as the solved region according to the center of any teeth of the radial. The solved region is shown as Fig.6, including the shaft, windings insulation and skeleton, coils, double-rotor core, PM.

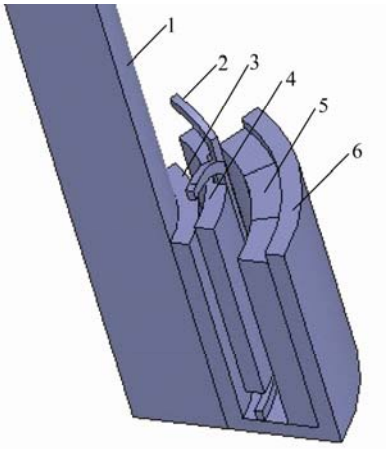

1. Shaft;
2. Coil;
3. Inner-rotor core;
4. Winding insulation and skeleton;
5. PM;
6. Outer-rotor core

Fig.6 Model of the prototype in temperature field

For the purpose of convenient calculation, the basic hypothesis and boundary conditions of the solved region are as follows:

The basic hypothesis for the prototype M/G in the transient temperature field:

1) Calculating the windings copper losses, considering the effect on each winding by the eddy current is the same, as that averaged;

2) Assuming the thermal source of stator iron losses does not change with temperature, but the winding heat source is only affected by time;

3) Assuming the windings end contacts with the skeleton surface, the heat source of the windings end is equal to the heat source of slot;

4) Ignoring the effect of pole arc coefficient on the transient temperature distribution.

The boundary conditions for the PM brushless M/G prototype in a temperature field:

1) Considering that the middle section of the axial center is an insulation surface, including double-rotor core, coils, windings skeleton, and the center section of PM. Due to the circumferential symmetry that considers the center section of slots as an insulation surface, including the stator windings skeleton, the center section of PM, which applies to the second convection heat transfer boundary conditions.

2) As to the outer surface of the outer-rotor and inner surface of the windings skeleton as the cooling surface, they apply to the third convection heat transfer boundary condition.

3) The top-face of the axis is a cooling surface; it applies to the room temperature boundary conditions.

The simulation result in the transient temperature field is shown in Fig.7, which indicates that the PM temperature is about 86 ℃ and below 115 ℃, which is the demagnetization temperature. Because the PM material of the prototype is NdFeB N35UH, its operating temperature is 180 ℃, so it will not cause the PM demagnetization. The temperature of the coils is below 125 ℃, and the insulation class of prototype is at H level, that is 180 ℃; the windings temperature rise is also in the range of normal operation. The average temperature curves of all objects are shown in Fig.8 from which it can be seen that the average temperature of the highest object is below 120 ℃. Through the FEA calculation in the transient temperature field under the normal operation condition in the natural environment, the prototype M/G temperature rise data is obtained. It provides guidance for the further optimal design. However, with the restriction of these kinds of hypothetical conditions and the effect of actual complex conditions, the losses need to be accurately calculated and comprehensively analyzed corresponding to the motor state, generator state, and maintenance state.

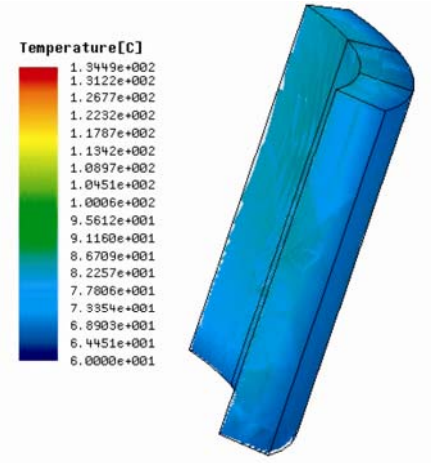

(a) The permanent magnet temperature field plot

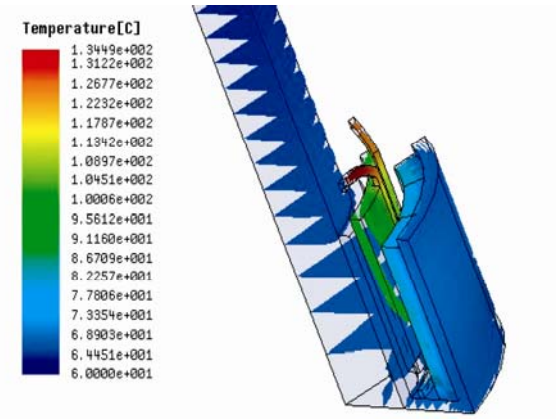

(b) All the Stators and rotors temperature field plot

Fig.7 Field plot in temperature field

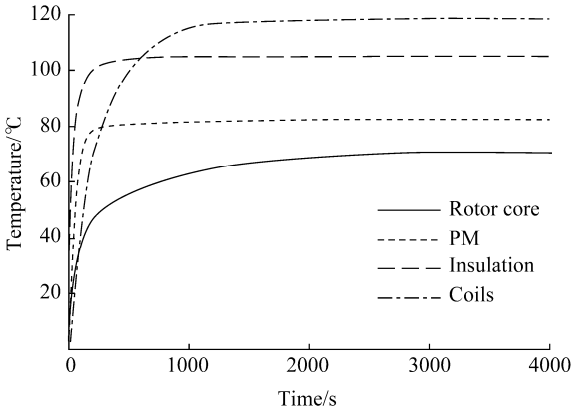

Fig.8 All objects average temperature curves in temperature field

5 Conclusions

In the magnetostatic field, transient field, and temperature field the FEA method was applied to calculate the reluctant structure Halbach PM brushless M/G which was proposed in this study. Through the simulation results the following conclusions can be safely drawn: 1) By the optimized design, the novel structure achieves the high speed, high power, and low losses of the design target; 2) The local overheating point is found under the normal operation condition, which benefits the advancement of the cooling effect; 3) The prototype M/G will further improve the efficiency of the electrical machine and strengthen the stability of the marine power system.

References

Ckdenas R, Peiia R, Ashe G, Clare J (2000). Control strategies for energy recovery from a flywheel using a vector controlled induction machine. *2000 IEEE 31st Annual Power Electronics Specialists Conference*, Galway, Ireland, 454-459.

Jang SM, You DJ, Ko KJ, Choi SK (2008). Design and experimental evaluation of synchronous machine without iron loss using double-sided Halbach magnetized PM rotor in high power FESS. *IEEE Transactions on Magnetics*, **44**(11), 4337-4340.

Jang SM, You DJ, Ko KJ, Choi SK (2009). Analysis on operational power and eddy current losses for applying coreless double-sided permanent magnet synchronous motor/generator to high-power flywheel energy storage system. *Journal of Applied Physics*, **105**(7), 105-107.

Kato S, Takaku T, Sumitani H, Shimada H (2009). Development of voltage sag compensator and UPS using a flywheel induction motor and an engine generator. *Electrical Engineering in Japan (English translation of Denki Gakkai Ronbunshi)*, **167**(1), 844-850.

Kohari Z (2009). Test results of a compact superconducting flywheel energy storage with disk-type permanent magnet motor/generator unit. *IEEE Transactions on Applied Superconductivity*, **19**(3), 2095-2098.

Park JD, Kalev C, Hofmann HF (2008). Control of high-speed solid-rotor synchronous reluctance motor/generator for flywheel-based uninterruptible power supplies. *IEEE Transactions on Industrial Electronics*, **55**(8), 3038-3046.

Rajapakshe A, Madawala UK, Muthumani D (2008). A model for a fly-wheel driven by a grid connected switch reluctance machine. *2008 IEEE International Conference on Sustainable Energy Technologies*, Singapore, 1025-1030.

Tang Pinghua (2009). Research on magnetic suspension flywheel electric machine for energy storage and control of drive system. PhD thesis, Harbin Institute of Technology, Harbin, 2-6. (in Chinese)

Tang Shuangqing (2003). Research on theory of magnetic suspension supporting system and application for flywheel battery. PhD thesis, Huazhong University of Science & Technology, Wuhan, 1-2. (in Chinese)

Upadhyay P, Mohan N (2009). Design and FE analysis of surface mounted permanent magnet motor/generator for high-speed modular flywheel energy storage systems. *Proceedings of the 2009 IEEE Energy Conversion Congress and Exposition*, San Jose, 3630-3633.

Wang Zhengguang (2008). Design of controlled system for flywheel driven device. Master thesis, University of Electronic Science and Technology, Chengdu, 9-13. (in Chinese)

Wasaki SD, Rajesh P, Liu Yong, Pride A, Zhu ZQ, James BJ (2009). Influence of PWM on the proximity loss in permanent-magnet brushless AC machines. *IEEE Transactions on Industry Applications*, **45**(4), 1359-1367.

Xi N, Sullivan CR (2009). An equivalent complex permeability model for litz-wire windings. *IEEE Transactions on Industry Applications*, **45**(2), 854-860.

Xia ZP, Zhu ZQ, Howe D (2004). Analytical magnetic field analysis of Halbach magnetized permanent magnet machines. *IEEE Transactions on Magnetics*, **40**(4), 1864-1872.

Yu Li, Cao Yongjuan, Liu Hexiang, Hu Qiansheng (2009). Design of a high efficiency generator/motor for flywheel energy storage system. *International Conference on Sustainable Power Generation and Supply*, Nanjing, 1- 3.

Yu Yali, Wang Yuanxi, Sun Feng (2011a). The latest development of the motor/generator for the flywheel energy storage system. *Proceedings 2011 International Conference on Mechatronic Science, Electric Engineering and Computer,* Harbin, 1228-1232.

Yu Yali, Wang Yuanxi, Sun Feng (2011b). Design of permanent magnet motor/generator using Halbach magnetized structure for the flywheel energy storage system. *Proceedings of the 6th International Forum on Strategic Technology,* Harbin, 593-597.

Zhu Deming, Yan Yangguang (2008). Features of air-gap flux density in segmented Halbach permanent magnet synchronous motor and its no-load EMF waveform optimization. *Transactions of China Electrotechnical Society*, **23**(11), 22-27.

Zhu ZQ，Howe D (2001). Halbach permanent magnet machine and applications: a review. *IEEE Proceedings of the Electronics*, **148**(4), 299-308.

Zhu ZQ, Xia ZP, Atallah K, Jewell GW, Howe D (2000). Analysis of anisotropic bonded NdFeB halbach cylinders accounting for partial powder alignment. *IEEE Transactions on Magnetics*, **36**(5), 3575-3577.

Yali Yu was born in 1978. She is a PhD candidate at the Department of Automation and a lecturer at Research Institute of Energy Storage Technology and Application, Harbin Engineering University. Her current research interests include special electrical machine, integrated electrical machine and comprehensive physical fields of electrical machine, *etc*.

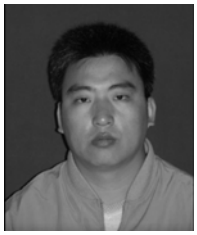

Yuanxi Wang was born in 1972. He is an engineer at Research Institute of Energy Storage Technology and Application, Harbin Engineering University. His current research interests include special electrical machine, integrated electrical machine and drive technology of electrical machine, *etc*.

Guosheng Zhang was born in 1964. He is an engineer at Research Institute of Energy Storage Technology and Application, Harbin Engineering University. His current research interests include special electrical machine, integrated electrical machine and mechanical manufacture of electrical machine, *etc*.

Feng Sun was born in 1944. He is a PhD advisor at Institute of Marine carrier device navigation equipment. His current research interests include Precision Instrument and Machinery, Measuring and Control Technology and Instruments and Navigation, Guidance and Control. He is an IEEE senior member, an editor board member of the Journal of Chinese Inertial Technology and a council member of the systems engineering and electronics. He has the nine Scientific and Technical awards. He is the major project leader of the Natural Science Foundation of China and the leader of many national plans and basic pre-research projects.